NJC

Accepted Manuscript

This is an *Accepted Manuscript*, which has been through the Royal Society of Chemistry peer review process and has been accepted for publication.

Accepted Manuscripts are published online shortly after acceptance, before technical editing, formatting and proof reading. Using this free service, authors can make their results available to the community, in citable form, before we publish the edited article. We will replace this *Accepted Manuscript* with the edited and formatted *Advance Article* as soon as it is available.

You can find more information about *Accepted Manuscripts* in the Information for Authors.

Please note that technical editing may introduce minor changes to the text and/or graphics, which may alter content. The journal's standard Terms & Conditions and the Ethical guidelines still apply. In no event shall the Royal Society of Chemistry be held responsible for any errors or omissions in this *Accepted Manuscript* or any consequences arising from the use of any information it contains.

ROYAL SOCIETY OF CHEMISTRY

www.rsc.org/njc

Journal Name

ARTICLE

Aerosol construction of multi-shelled $LiMn_2O_4$ hollow microspheres as a cathode in lithium ion batteries

Received 00th January 20xx,
Accepted 00th January 20xx

DOI: 10.1039/x0xx00000x

www.rsc.org/

Xiaofeng Niu,[a] Yunfeng Li,[ab] Yanjie Hu,*[a] Hao Jiang,[a] Xiaoyu Hou,[a] Wenge Li,[a] Shengjie Qiu,[b] and Chunzhong Li *[a]

Advanced cathode materials with the optimal balanced pores structures and tap density have attracted more attention for next generation lithium ion batteries (LIBs). Herein, the multi-shelled $LiMn_2O_4$ hollow microspheres (named as ms-LMO HMs) have been successfully prepared by a facile aerosol spray pyrolysis route through the controlled combustion of carbon species. The obtained microspheres with diameters of 0.5 - 2 μm are assembled by nanosized $LiMn_2O_4$ particles (10 - 30 nm) and exhibit intriguing hollow structures with multi shells. When used as cathode materials in LIBs, the ms-LMO HMs show a superior specific capacity of 110 mA h g^{-1} with 400 cycles at 0.2 A g^{-1}, as well as a good rate capacity. This is mainly owing to the multilevel voids, porous internal/extra shells and nanosized particles for the easily wetting of electrode and electrolyte, and facilitated Li^+ ions diffusion pathway.

1. Introduction

Advanced cathode materials have been regarded as a key important component for lithium ion batteries (LIBs) with high energy and power density.[1-3] Spinel $LiMn_2O_4$ has been deemed to be one of the most competitive cathode materials to substitute for commercial $LiCoO_2$ owing to its advantages of high theoretical capacity (148 mA h g^{-1}), outstanding voltage profiles (3.0-4.5V), good safety, low toxicity, rich and cheap resource, and eco-friendly.[4-7] However, during the charge-discharge cycles, long distance of Li^+ diffusion in bulk $LiMn_2O_4$ leads to the serious polarization of the cathode materials, which results in a rapid fading capacity and poor rate performance in practical applications[8-9].

Many strategies have been developed to solve the above mentioned problems, for instance, designing electrode materials at nanoscale and constructing effective structures.[10-11] The nanosized assembled units possess significantly shorten diffusion distances and highly effective interfacial areas between electrode and the electrolyte for Li^+ ions, which is significantly beneficial to the improvement of the rate capacity ability in LIBs.[12-17] On the other hand, among these designed nanostructures such as nanoparticles, nanorods, nanowires, and so on,[16-19] hollow $LiMn_2O_4$ microspheres assembled of nanosized particles have attracted more attention due to their large surface area and interior hollow structures as well as active components at nanoscale, which facilitates the directly contact of electrolyte and electrode, as well as the diffusion of Li^+ ions during the charge-discharge process.[20-21] Hollow $LiMn_2O_4$ microspheres with high specific surface area of 17.5 m^2/g have been synthesized by lithiating MnO_2 hollow microspheres and exhibited the discharge capacity of 110 mA h g^{-1} at a current density of 100 mA g^{-1} after 55 cycles.[22] Zhou et al designed $LiMn_2O_4$ microspheres with adjustable hollow void through the conversion of porous MnO_2 microspheres in solution and these hollow microspheres as cathode materials showed a high capacity retention rate of 96.6 % after 105 cycles at 140 mA g^{-1} (the initial capacity: 113.9 mA h g^{-1}).[23] However, for these hollow microspheres, more voids form interior hollow structures do not facilitate the improvement of specific capacity due to the lowered tap density though there exists conveniently interfacial contacting pathways for electrode, the electrolyte and Li^+ ions. Therefore, it is still a challenge for the optimization balance of controlled voids and the utilization of active $LiMn_2O_4$ components.

Recently, yolk-shell microspheres have been demonstrated to be an effective hierarchical structure for the balanced design of adequate voids for the volume change and more electrochemical active species from the shells and yolk cores.[24] Qiao et al. prepared yolk-structured $LiMn_2O_4$ microspheres from the yolk-shell $MnCO_3$-MnO_2 template by multi-step procedures and high discharge capacity of 128.9 mA h g^{-1} at 74 mA g^{-1} after 100 cycles and excellent rate capacity are obtained because of a balance between the high surface area and good mechanical stability.[25] $LiMn_2O_4$ as well as

[a]*Key Laboratory for Ultrafine Materials of Ministry of Education, School of Materials Science and Engineering, East China University of Science & Technology, Shanghai 200237, China. E-mail: czli@ecust.edu.cn (Prof. C. Li) and huyanjie@ecust.edu.cn (Prof. Y. Hu); Fax: +86 21 64250624; Tel: 86- 21- 6425-0949.*
[b]*Shanghai Nanotechnology Promotion Center, Shanghai 200237, China*
Electronic Supplementary Information (ESI) available: SEM images of $LiMn_2O_4$-C precursor microspheres, HR TEM images, TG and DSC profiles, Nitrogen adsorption/desorption isotherm, coulombic efficiency profiles of the ms-LMO HMs.

$LiNi_{0.5}Mn_{1.5}O_4$ yolk-shell powders exhibited a unique filled-core@void@shell configuration and displayed superior electrochemical performance compared to the dense spheres.[26-27] However, the internal dense yolks have a similar morphology of solid microspheres, which not facilitated for the diffusion of Li^+ ions and the penetration of electrolyte. And the corresponding preparing processes are multi-step, complex and time-consuming. Therefore, it is urgently need to develop a simple and controlled method to synthesize more efficient $LiMn_2O_4$ hierarchical nanostructures for LIBs.

Herein, multi-shelled $LiMn_2O_4$ hollow microspheres (ms-LMO HMs) have been prepared by a facile aerosol ultrasonic spray pyrolysis approach with sucrose as structure-direction agent, followed by the post calcination in air. These microspheres are assembled by $LiMn_2O_4$ nanosized particles with unique particle-particle interaction and have unique shell-void-shell-void-shell-viod structures. When used as cathode materials for LIBs, the ms-LMO HMs shows a superior specific capacity and excellent cyclic stability.

2. Experimental section

2.1 Synthesis of the ms-LMO HMs

For the preparation of ms-LMO HMs, a precursor solution was prepared by dissolving lithium acetate dehydrate ($CHCOOLi{\cdot}2H_2O$, AR, Sinopharm Chemical Reagent Co., LTD) and manganese acetate tetrahydrate ($(CHCOO)_2Mn{\cdot}2H_2O$, AR, Sinopharm Chemical Reagent CO., LTD) in distilled water with a Li/Mn molar ratio of 1:2. And the over 5 % lithium source was added to facilitate the formation of $LiMn_2O_4$. The total concentration of Li^+ and Mn^{2+} was 0.2 M and 0.4 M sucrose (AR, Shang Hai Ling Feng Chemical Reagent CO., LTD) was employed as structure-direction agent for the construction of targeted materials. Then the solution containing Li^+, Mn^{2+} and sucrose was injected into an ultrasonic atomization generator (1.7 MHz) to produce droplets, which were subsequently carried into a high-temperature quartz-tube reactor (inner diameter: 60 mm, length: 800 mm) with temperature of 800 °C by a carrier air of 500 L h^{-1}. The powders were prepared through the pyrolysis of droplets and collected on a glass fiber filter (GA-55, Japan) with an aid of vacuum pump. Finally, the ms-LMO HMs was obtained after further calcination at temperature of 600 °C for 3 h with heating rate 2.5 °C min^{-1} in a muffle furnace with air atmosphere. Meanwhile, the dense LMO spheres were also prepared by the same process just without the template of sucrose.

2.2 Characterization

The morphology and structure of the ms-LMO HMs were checked out using filed emission scanning electron microscopy (FE-SEM: HIACHI-S4800), and transmission electron microscope (HRTEM: JEOL JEM-2100). The crystal composition was tested using X-ray diffraction (XRD: D/max 2550V). The surface chemical state was investigated with X-ray photoelectron spectroscopy (XPS: ESCALAB 25). Nitrogen adsorption-desorption (Micromeritics ASAP 2460) was tested by the Brunauer-Emmett-Teller (BET) method. The heat change of the powder was measured using thermogravimetric analysis (TG: NETZSCH STA409PC).

2.3 Electrochemical measurements

The working electrode was consisted of 70 % active materials (ms-LMO HMs), 15 % conductive materials (acetylene black) and 15 % binder (polyvinyldifluoride, PVDF), all of these three materials were mixed with a certain amount of N-methyl-2-pyrrolidone (NMP) and stirred over 12 h. Then the mixtures were pasted on aluminum foil with a 50 μm thickness. Lithium metal (ϕ 16×1.2 mm) was used as anode while polypropylene membrane (Celgard 2400) was used as separator between cathode and anode, respectively. The electrolyte was a mixture of 1 M $LiPF_6$ and ethylene carbonate - dimethyl carbonate (EC-DMC) and the volume ratio of EC-DMC was 1:1. The electrochemical measurements were determined by 2016-type coin half cell. The cell was assembled with the help of glove box (Mikrouna Advanced Series), which could isolated water and oxygen through filled with high-purity Ar (99.999%). The cycle performance was tested by LAND-CT2001C test system. The cyclic voltammograms (CV) was measured by electrochemical workstation (Autolab PGSTAT302N).

3. Results and discussion

3.1 Phase composition and morphology

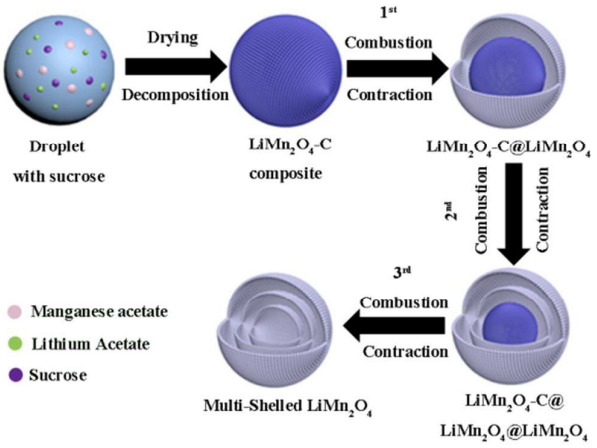

Fig. 1 Illustration of the formation of the ms-LMO HMs in a aerosol process with sucrose as direction agents.

Fig. 1 shows the corresponding formation mechanism of the ms-LMO HMs. Firstly, the microsized precursor droplets produced by ultrasonic atomization generator were carried into quartz reactor with a constant high temperature. Then, the vaporization of water as well as decomposition of metal salts and sucrose mixture occurred during the short heating time for obtaining a mixture of carbon and metal oxide precursor spheres. Subsequently, in the calcination process, the combustion of carbon took place firstly in the surface of microspheres but not inside because of the inadequacy of oxygen, which is a necessary oxidant for carbon combustion. Thus, the inner unburned mixture microspheres contracted

owing to the drastic temperature difference between the surface and inner. Finally, a special core@void@shell configuration was formed with $LiMn_2O_4$ shell and carbon mixed oxide core parts, as well as void between them under this condition. Similarly, a following second combustion of carbon would take place in the surface of carbon mixed oxide core and a second contraction occurred for the formation of core@void@shell configuration. That is to say, the configuration of core@void@shell@void@shell was formed after second combustion. In the last, sufficient calcination with three or more times combustion and contraction transformed the core into hollow nanosphere with mutishells, and then ms-LMO HMs was obtained. Obviously, it was no doubt that addition of sucrose into the precursors solution played a key role in the formation of the ms-LMO HMs.

Fig 2 shows the XRD patterns of as-prepared $LiMn_2O_4$-C precursor spheres and ms-LMO HMs after the calcination. Obviously, The $LiMn_2O_4$-C precursor microspheres obtained by one-step ultrasonic spray pyrolysis process have weak diffraction peaks of standard $LiMn_2O_4$ (PDF #35-0782), indicating that worse crystalline characteristics. This is mainly attributed to the extremely short reaction residence time for the further crystal growth. The widely weak patterns at 2θ = 20 - 30° suggest that the existence of the amorphous carbon and residual sucrose. For the multi-level hollow structures as well as improved crystallinity, post calcinations treatment had been employed. As shown in **Fig 2**, the distinct diffraction peaks were detected in XRD, which are well matched with spinel $LiMn_2O_4$ (PDF #35-0782). The sharp patterns demonstrate that the obtained ms-LMO HMs exhibits a high crystallinity and the wide peaks in a range of 2θ = 20 - 30° indicate that the microspheres are composed of nanosized $LiMn_2O_4$ particles. After the calculation by the Scherrer equation,[28] it is noted that the average crystal size of 31 nm is obtained for the ms-LMO HMs, which can provide a facilitated pathway for the diffusion of Li^+ ions.[26]

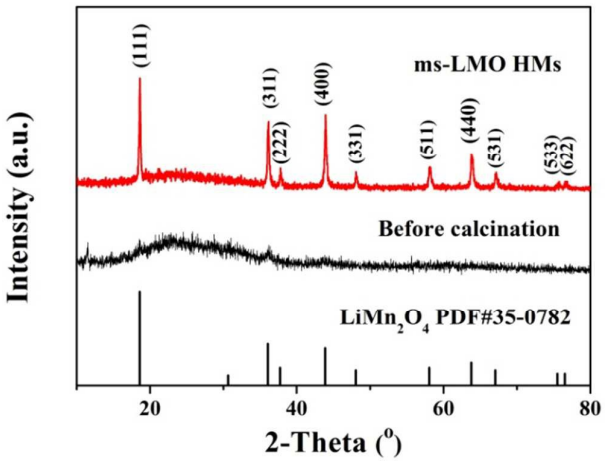

Fig. 2 XRD patterns of as-prepared $LiMn_2O_4$-C precursor spheres and ms-LMO HMs after the calcination.

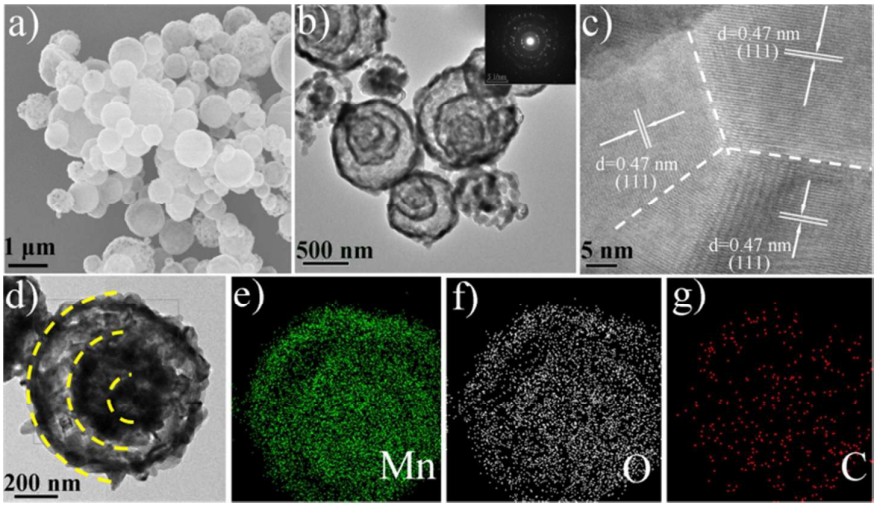

Fig. 3 (a) SEM and (b) TEM image of as-synthesized ms-LMO HMs, (c) HRTEM image of particle-particle interaction in ms-LMO HMs, and (d) TEM image of a single sphere, and (e-g) the corresponding element mapping images.

Fig. 3a depicts the SEM image of the obtained ms-LMO HMs. A relatively uniform spherical shape are clearly observed and these microspheres have diameters in range of 0.5 - 2 μm. The rough surface morphologies with pores observed are significantly different from that of the prepared $LiMn_2O_4$-C precursor spheres (SEM images in **Fig. S1.†**) and dense $LiMn_2O_4$ without sucrose (SEM images in **Fig. S2a.†**). The results demonstrate that post calcination procedures play a key role for improving the crystallinity and the formation of unique hollow structures derived from the further combustion of carbon species (as illustrated in **Fig. 1**). The TEM image of the ms-LMO HMs is shown in **Fig. 3b**. Obviously, these microspheres possess multi $LiMn_2O_4$ shells and have a clear shell@void@shell@void@shell configuration. Which is different with the obtained dense LMO spheres without an assistance of sucrose (TEM images in **Fig. S2b†**). And the shells

are porous and assembled by nanosized $LiMn_2O_4$ particles with diameters of 10 - 30 nm (**Fig. S3**†), which is in a good agreement with the XRD results. The selected-area electron diffraction (SAED) pattern (the inset in **Fig. 3b**) indicates the polycrystalline nature and further demonstrates the presence of nanosized particles in the ms-LMO HMs. It is worth mentioning that there exists a strong particle-particle interaction among the $LiMn_2O_4$ primary particles in the ms-LMO HMs. As shown in **Fig. 3c**, the distinct interface with a strong contacting interaction are characterized by the HRTEM image owing to the matched orientation growth of $LiMn_2O_4$ crystals in a high-temperature calcination process. More, the clear interplanar spacing (0.47 nm) of lattice fringes is identified, which relates to the (111) plane of spinel $LiMn_2O_4$ and further indicates the high crystallinity. **Fig. 3d-g** depicts the detailed information of Mn, O, and C elements in a single ms-LMO HMs, indicating the uniform distribution. Notably, the trace of carbon is found in **Fig. 3g** and it is mainly ascribe to the partial oxidation of sucrose and some carbon species even at temperature of 600 °C for 3 h with air atmosphere. The content of carbon can be calculated to be 3.38 wt% by the TG analysis (**Fig. S4.**†). The doping of few carbon plays a positive effect for the enhancement of the conductivity of $LiMn_2O_4$ cathode materials, which could improve the specific capacity and rate performance of electrode materials.[29] The corresponding specific surface area is measured to be 13.5 $m^2 g^{-1}$ and the formation of the 4 - 10 nm mesopores are also identified because of the aggregations among the nanosized $LiMn_2O_4$ particles (**Fig. S5.**†). Compared to the dense LMO spheres, these unique mesopores and voids in the ms-LMO HMs could provide flexible pathways for the Li^+ ions diffusion and easily wetting of active electrode and electrolyte.[30]

The chemical state of the surface elements in the ms-LMO HMs is investigated by XPS in detail, as shown in **Fig. 4**. It is noted that the sharp peaks of C1s, O1s and Mn2p are depicted in **Fig. 4a**. The Mn2p peak fitted spectra is given in **Fig. 4b**, which is mainly the peak of $Mn2p_{1/2}$ and $Mn2p_{3/2}$. As known, the average chemical valence of Mn in $LiMn_2O_4$ is + 3.5 and the peak ($Mn2p_{3/2}$) at 637.0 - 647.0 eV can be divided into two typical peaks, which corresponds to Mn^{3+} (641.5 eV) and Mn^{4+} (642.8 eV) in Mn_2O_3 and MnO_2 structures, respectively. The presence of Mn^{3+} and Mn^{4+} in the ms-LMO HMs is consistent with the literature reported.[31]

3.2 Electrochemical performance

The electrochemical properties of ms-LMO HMs are shown in **Fig. 5. Fig. 5a** gives the CV profiles of initial three cycles with the scan rate of 0.2mV s^{-1} while the voltage range is from 3.2V to 4.4V. The peak appears at 3.25 V during the first positive sweep but disappears later, is corresponded to the plateaus around 3.2V, who can cause Jahn-Teller and followed result in capacity decay irreversibly. The open- circuit potentials of the as-prepared half-cells are ranged from 2.8-2.9V, so the 3.25 V plateaus would contribute some capacity when the cell was charged or first time, but it doesn't occur during the discharged process and the following cycles owing to the termination of the voltage at 3.3V. The cathodic peaks at 3.92V and 4.04V are well related to Li^+ intercalation into the

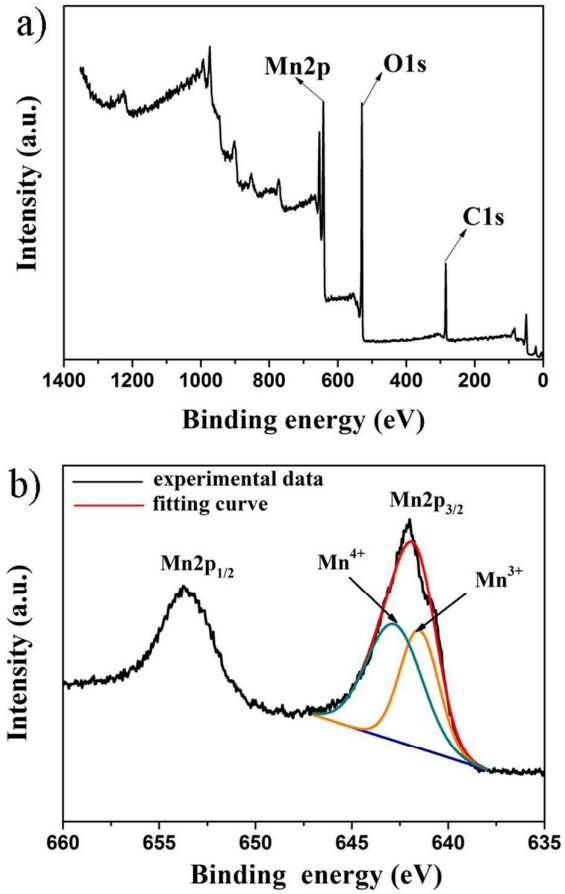

Fig. 4 XPS profiles of ms-LMO HMs: (a) general spectrum, and (b) $Mn2p_{3/2}$ peaks.

oxide, and the anodic peaks at 4.08V and 4.21V are corresponded to deintercalation of Li^+,[32] the overlapped of the three curves prove that the ms-LMO HMs have an excellent cycle reversible electrochemical process during intercalation / deintercalation of Li^+. **Fig. 5b** gives the charge and discharge profiles at selected cycles. There are two voltage plateaus around 4.0V and 4.1V, corresponding to two phase transform during cycle. The result is well matched with cathodic and anodic peaks in **Fig. 5a**. Furthermore, the initial charge capacity is 145.2 mA h g^{-1}, while discharge capacity is 110mA h g^{-1}, the first Coulombic efficiency reaches only 75.2%, the phenomenon can be explained by the existence of the plateaus at 3.25 V mentioned in the CV curves. After several cycles, the discharge capacity is stayed around 119 mA h g^{-1}. The result is well in agreement with the overlapped of the CV curves of **Fig. 5a**.

The cycle performances and Coulombic efficiency of ms-LMO HMs and dense LMO are shown in **Fig. 5c** and **Fig. S6**. The discharge capacity of LMO without sucrose is 87.7 mA h g^{-1} in the initial cycle, and it remains 75.6 mA h g^{-1} after 400 cycles with a capacity retention rate of only 86.2%. However, the discharge capacity of ms-LMO HMs is 110mA h g^{-1} in the initial

cycle and remains 101.1 mA h g^{-1} after 400 cycles with a higher capacity retention rate up to 91.9%. Either discharge capacity or cycle stability of ms-LMO HMs is better than that of dense LMO prepared without sucrose. Meanwhile, the ms-LMO HMs exhibit higher Coulombic efficiency of 99.6% after 400 cycles than that (98.3%) of dense LMO electrode. The good cycle stability and high Coulombic efficiency is due to the aggregations among the nanosized $LiMn_2O_4$ particles, as well as unique mesopores and voids in the ms-LMO HMs. The detailed structure of the ms-LMO HMs electrode after 400 cycles has been characterized by TEM (Inset of **Fig. 5c** and **Fig. S7.†**). It is clearly noted that the active materials after 400 cycles maintain perfect spherical and multi-shelled structures owing to the unique aggregations among the nanosized $LiMn_2O_4$ particles. Meanwhile, the mesopores and voids provide a shorten Li^+ diffusion distance and achieve easier contact between electrode and electrolyte. These reasons result in good electrochemcial performances in capacity retention, stability and rate ability. Moreover, the existence of carbon, identified by element mapping and TG, could enhance the conductivity of $LiMn_2O_4$ cathode materials, very helpful to improve the stability and rate ability of the cycle. The rate performance of ms-LMO HMs and LMO without sucrose are displayed in **Fig. 5d**. When the discharge rate was ranged from 0.1 to 0.2, 0.4, 0.6, 0.8, 1.0 A g^{-1}, the discharge capacity of ms-LMO HMs changed from 106.8 to 106.5, 105.6, 106.2, 101.1, 94.7 mA h g^{-1}, respectively. As a contrast sample, it is seen that the specific capacity changed from 80.3 to 80.1, 71.5, 60.4, 47.3, 30.8 mA h g^{-1} for LMO without sucrose at different current density. It is worth to say that, the discharge capacity of ms-LMO HMs is 206% higher than dense LMO When tested in 1.0 A g^{-1}, much worse than those of ms-LMO HMs. The slightly decrease of capacity with increasing currents indicate good rate performance of ms-LMO HMs electrode, which is ascribed to the doping of carbon in ms-LMO HMs, which can improve the conductivity of integral ms-LMO HMs electrode .The outstanding cycling stability and superior rate performance is attributed to the following three aspects: 1) shorter lithium ion diffusion paths constructed by the multi-shell hollow structure; 2) easier contacts between electrode and electrolyte in the voids of ms-LMO HMs; 3) carbon doping of the shells for enhanced electrical conductivity.

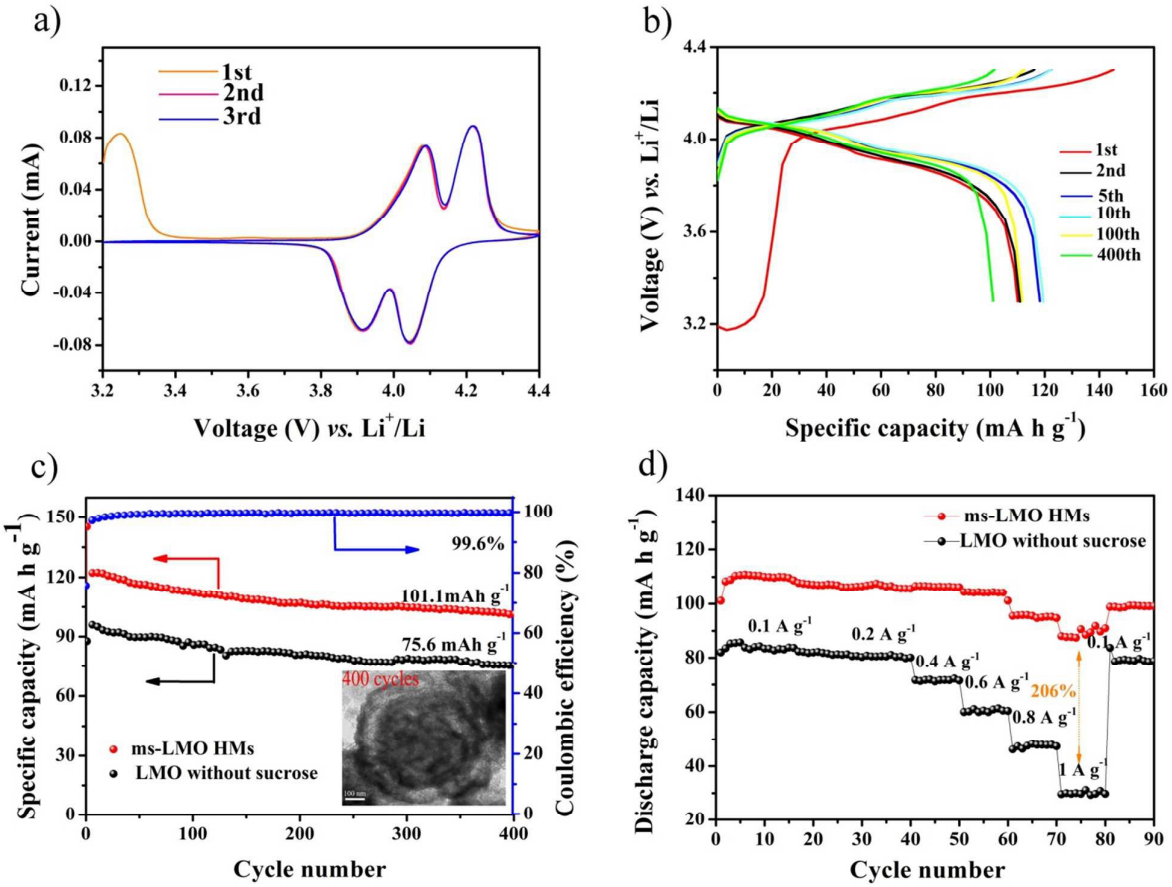

Fig. 5 (a) Cycle voltammograms of the initial three cycles in the voltage range from 3.2 - 4.4 V, (b) Charge and discharge profiles at selected cycles from 3.3 V - 4.3 V with the current density of 0.2 A g^{-1}, (c) Cycle performance of ms-LMO HMs and LMO without sucrose at 0.2 A g^{-1}, and Coulombic efficiency of ms-LMO HMs and inset TEM images of ms-LMO HMs electrode after 400 cycles (d) Rate performance of ms-LMO HMs and LMO without sucrose measured by different current densities of 0.1 A g^{-1} to 1 A g^{-1}.

Journal Name

ARTICLE

4. Conclusions

In summary, the multi-shelled $LiMn_2O_4$ hollow microspheres have been successfully prepared by a facile ultrasonic spray pyrolysis route followed by post calcination treatment. These microspheres have diameters of 0.5 - 2 μm and exhibit intriguing hollow structures with multi shells, which are assembled by nanosized $LiMn_2O_4$ particles of 10 - 30 nm with a strong particle-particle interaction. In an aerosol process, the controlled combustion of carbon species plays important part in the formation of unique hollow structures. When used as cathode in LIBs, the multi-shelled $LiMn_2O_4$ hollow microspheres show a high specific capacity of 110 mA h g^{-1} with a high capacity retention up to 91.9% after 400 cycles with a current density of 0.2 A g^{-1}, as well as a good rate performance. The superior electrochemical performance is attributed to the multilevel voids, porous internal/extra shells and nanosized particles, which provide an excellent platform for the easily wetting of electrode and electrolyte, facilitated Li^+ ions diffusion and a relative high tap density of active materials. It is further noted that the assembly in aerosol process is an effective protocol for the design and construction of advanced hierarchical electrode materials for LIBs.

Acknowledgements

This work was supported by the National Natural Science Foundation of China (21236003, 21371057), the Basic Research Program of Shanghai (14JC1490700), the Research Project of Chinese Ministry of Education (113026A), the Shanghai Shuguang Scholars Program (13SG31), Project funded by China Postdoctoral Science Foundation (2014M 561497) and the Fundamental Research Funds for the Central Universities.

Notes and references

1 M. J. Lee, S. H. Lee, P. Oh, Y. S. Kim and J. Cho, *Nano Lett.*, 2014, **14**, 993.
2 F. Wu, N. Li, Y. F. Su, L. J. Zhang, L. Y. Bao, J. Wang, L. Chen, Y. Zheng, L. Q. Dai, J. Y. Peng and S. Chen, *Nano Lett.*, 2014, **14**, 3550.
3 L. Chen, Y. F. Su, S. Chen, N. Li, L. Y. Bao, W. K. Li, Z. Wang, M. Wang and F. Wu, *Adv. Mater.*, 2014, **26**, 6756.
4 S. H. Lee, M. S. Jeong and J. Cho, *Adv. Energy Mater.*, 2013, **3**, 1623.
5 S. H. Lee, G. B. Yoon, M. S. Jeong, M. J. Lee, K. Kang and J. Cho, *Angew. Chem. Int. Ed.*, 2014, **53**, 1.
6 D. C. Tang, Y. Sun, Z. Z. Yang, L. B. Ben, L. Gu and X. J. Huang, *Chem. Mater.*, 2014, **26**, 3535.
7 H-W. Lee, P. Muralidharan, R. Ruffo, M. C. Mari, Y. Cui, D. K. Kim, *Nano Lett.,* 2010, **10**, 3582.
8 Y. J. Liu, J. Lv, Y. Fei, X. D. Huo and Y. Z. Zhu, *Ionics*, 2013, **19**, 1241.
9 Y. H. Wang, L. Chen, Y. G. Wang, Y. Y. Xia, *Electrochim. Acta*, 2015, **173**, 178.
10 K. X. Wang, X. H. Li and J. S. Chen, *Adv. Mater.*, 2015, **27**, 527.
11 M. J. Armstrong, C. O. Dwyer, W. J. Macklin and J. D. Holmes, *Nano Res.*, 2014, **7**, 1.
12 D. Luo, G. S. Li, C. C. Fu, J. Zheng, J. M. Fan, Q. Li and L. P. Li, *Adv. Energy Mater.*, 2014, DOI: 10.1002/aenm.201400062.
13 Y. C. Du, X. S. Zhu, X. S. Zhou, L. Y. Hu, Z. H. Dai and J. C. Bao, *J. Mater. Chem. A,* 2015, **3**, 6787.
14 Y. C. Du, X. S. Zhu, L. Si, Y. F. Li, X. S. Zhou and J. C. Bao, *J. Phys. Chem. C*, 2015, **119**, 15874.
15 H. Zhang, Y. L. Xu and D. Liu, *RSC Adv.*, 2015, DOI: 10.1039/c4ra13041c.
16 Y. J. Cai, Y. D. Huang, X. C. Wang, D. Z. Jia, W. K. Pang, Z. P. Guo, Y. P. Du and X. C. Tang, *J. Power Sources*, 2015, **278**, 574.
17 D. Zhan, Y. Liang, P. Cui and Z. A. Xiao, *RSC Adv.*, 2015, **5**, 6372
18 C .Z. Li, Y. J. Hu and W. K. Yuan, *Particuology*, 2010, **8**, 556.
19 S. Y. Lee, Y. S. F. Oshima, E. J. Hosono, H. S. Zhou, K. S. Kim, H. S. M. Chang, R. J. Kanno and K. Takayanagi, *ACS Nano*, 2015, **9**, 626.
20 C. Y. Zhu, G. K. Saitoa and T. Akiyama, *J. Mater. Chem. A*, 2013, **1**, 7077.
21 J. Qi, X. Y. Lai, J. Y. Wang, H. J. Tang, H. Ren, Y. Yang, Q. Jin, L. J. Zhang, R. B. Yu, G. H. Ma, Z. G. Su, H. J. Zhao and D. Wang, Chem. Soc. Rev., 2015, DOI: 10.1039/c5cs00344j.
22 X. L. Xiao, J. Lu and Y. D. Li, *Nano Res.*, 2010, **3**, 733.
23 L. Zhou, X. F. Zhou, X. D. Huang, Z. P. Liu, D. Y. Zhao, X. D. Yao and C. Z. Yu, *J. Mater. Chem. A*, 2013, **1**, 837.
24 Y. J. Hong, M. Y. Son and Y. C. Kang, *Adv. Mater.*, 2013, **25**, 2279.
25 Y. Qiao, S. R. Li, Y. Yu and C. H. Chen, *J. Mater. Chem. A*, 2013, **1**, 860.
26 C. M. Sim, S. H. Choi and Y. C. Kang, *Chem. Commun.*, 2013, **49**, 5978.
27 S. H. Choi, Y. J. Hong and Y. C. Kang, *Nanoscale*, 2013, **5**, 7867.
28 J. H. Frantti and Y. K. Fujioka, *Ann. Phys.*, 2015, **527**,219.
29 M. X. Tang, A. B. Yuan and J. Q. Xu, *Electrochim. Acta*, 2015, **166**, 244.
30 S. Q. Liang, J. Yi and A. Q. Pan, *Int. J. Electrochem. Sci.*, 2013, **8**, 6535.
31 M. S. Jeong, M. J. Lee, J. Cho and S. H. Lee, *Adv. Energy Mater.*, 2015, DOI: 10.1002/aenm.201500440.
32 X. Zhao, M. V. Reddy, H. X. Liu, S. Ramakrishna, G. V. S. Rao and B. V. R. Chowdari, *RSC Adv.*, 2012, **2**, 7462.

Graphic Abstract

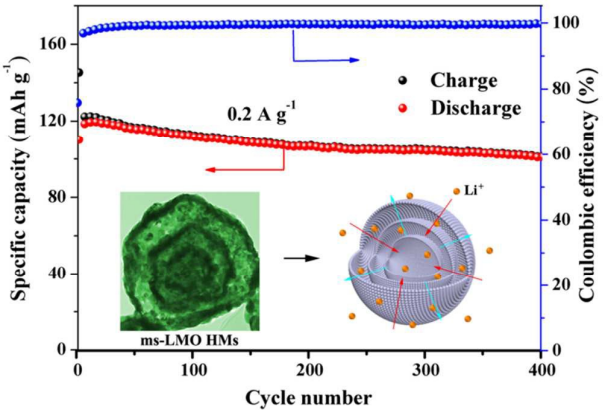

Novel multi-shelled $LiMn_2O_4$ hollow microspheres have been successfully prepared by a facile aerosol spray pyrolysis route through the controlled combustion of carbon species. These microspheres show a superior specific capacity good rate capacity when as cathode materials in LIBs.